European Polymer Journal 148 (2021) 110338

Contents lists available at ScienceDirect

European Polymer Journal

journal homepage: www.elsevier.com/locate/europolj

Flexible acrylic-polyurethane based graft-interpenetrating polymer networks for high impact structural applications

Nima Alizadeh [a,b], Eldon Triggs [b,c], Ramsis Farag [a,d], Maria L. Auad [a,b,*]

[a] Department of Chemical Engineering, Auburn University, United States
[b] Center for Polymers and Advanced Composites, Auburn University, United States
[c] Department of Aerospace Engineering, Auburn University, United States
[d] Department of Textile Engineering, Mansoura University, Egypt

ARTICLE INFO

Keywords:
Graft-interpenetrating polymer networks
Polyurethane
Acrylic-based copolymers
Viscoelastic properties
Impact resistance
Elastomeric materials
Adhesives

ABSTRACT

Flexible graft-interpenetrating polymer networks (IPNs) were synthesized out of polyurethane (PU) and acrylic-based copolymers using two co-monomers, styrene and methyl methacrylate (MMA). Chemical bonds between the two polymers participating in the interpenetration network were utilized to decrease the system's phase separation. The effect of changing the composition of the two co-monomers on the properties of the IPN system was studied. Dynamic mechanical analysis (DMA), tensile, and shear tests were used to characterize the thermomechanical and mechanical properties of IPNs sheets/plates and IPNs as an adhesive. A scanning electron microscope (SEM) was utilized to characterize the failure mechanism of the tensile dog bone samples. Moreover, impact tests were performed on a sandwich structure with synthesized IPN as an inter-layer adhesive to characterize the toughness and stiffness of the IPN samples. Overall, excellent transparency and impact resistance in visible light range with a wide range of thermo-mechanical properties (from extreme elastomeric to more ductile) was observed in IPN samples, which shows their tremendous potential in various transparent, high-performance applications.

1. Introduction

Transparent impact-resistant materials can be used in different applications such as electronic devices, windshields, protecting enclosures [1], canopies [2], and many general applications. Excellent transparency, impact resistance, ballistic resistance, and low density are some of the essential features which each transparent protective material should have. Sands et al. indicated that, while transparent protective materials cover just 15% of the whole surface of body armors, they contribute to 30% of the entire weight of body armor [3].

Traditionally, bulletproof glass (laminated glass) was used in high-performance transparent applications. Laminated glasses consist of a couple of glass layers with plastic layers between them [4]. Plastic layers with high toughness could withstand the harsh projectile and make the whole system impact resistance. However, laminated glasses lose their transparency after experiencing several strikes [5]. Transparent ceramics, which have better thermomechanical properties, are other options for the high-performance transparent application [6]. Nonetheless, the manufacturing process, price, and availability are the most important disadvantages of ceramics [5].

The recent transparent protective materials consist of three layers, a hard strike face, an intermediate layer, and a backing layer called a "spall" layer. The strike face is disturbing the energy, while the intermediate layer objection is absorbing the energy. Finally, the spall layer prevents outer and intermediate fractured layers from spraying or "spalling" into the passenger compartment or inside layer [7]. These layers stick to each other by an adhesive interlayer, usually manufactured from polyurethanes (PUs) [7]. Transparent protective materials are taking much attention due to their unique properties [8]. Acrylates such as Plexiglas® and polycarbonates (PC) such as Lexan® are two main groups of amorphous polymers used for transparent impact resistant applications [5]. Amorphous polymers are mostly used in the intermediate and adhesive interlayer, where low density and transparency are critical [7]. However, PC, for instance, has low ultraviolet light (UV) resistance, chemical resistance, scratch resistance, and high price [9]. Vinyl ester resins (VER) such as bisphenol-A based dimethacrylate resins are widely used in military, high-performance applications, and as a matrix in composites due to the excellent thermomechanical properties

* Corresponding author at: Department of Chemical Engineering, Auburn University, United States.
E-mail address: auad@auburn.edu (M.L. Auad).

https://doi.org/10.1016/j.eurpolymj.2021.110338
Received 13 November 2020; Received in revised form 27 January 2021; Accepted 3 February 2021
Available online 15 February 2021

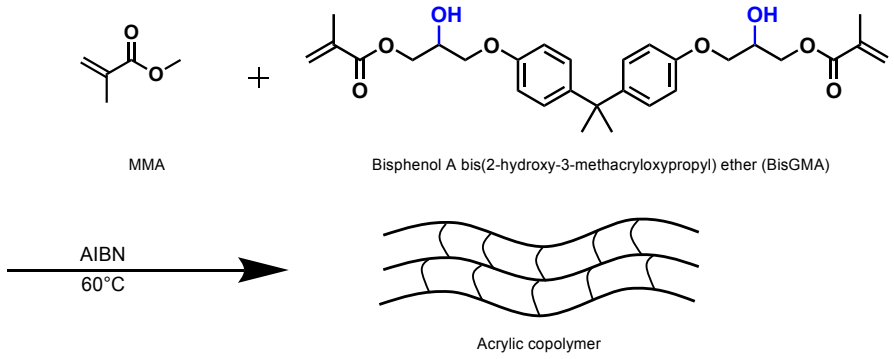

Fig. 1-a. Free radical polymerization of acrylic copolymer out of MMA and BisGMA.

[10–12]. However, due to high viscosity, mostly lower viscosity co-monomers such as styrene, which has excellent transparency and low price, and methyl methacrylate (MMA) are mixed with the vinyl ester resins to increase processability [11,13]. Poly(methyl methacrylate) (PMMA) is an amorphous polymer widely used in transparent applications due to the high similarity to glass [7]. Chemical resistance, wearing resistance, ease of processability, relatively high stiffness, and UV resistance are some of the desirable properties of PMMA in high-performance transparent applications [7].

Since VER resins are brittle, blending with rubbery materials such as PU is required to increase the toughness [14]. PU is an elastomeric material with high impact resistance better than PC. PU has tailorable properties that make it a great candidate in various applications, including protective applications [15,16]. The choice of the molecular weight of monomers, catalysts, chemical configuration of isocyanate, and the synthesis method affect the final morphology of PU [17], therefore changing the structural properties [17–19].

Blending polymers is considered one method to enhance the desirable properties for specific applications [20,21]. However, blending polymers has its challenges due to the low entropy of mixing in big molecules [22,23]. Different methods such as copolymerization, grafting, and interpenetrating polymer networks (IPNs) were introduced to solve the immiscibility of the polymers [24,25].

IPNs include two polymers where both networks are physically entangled, and it is not possible to separate them without breaking their bonds [25]. IPNs are classified as semi-IPN, full-IPN, and graft-IPN based on their structure. Semi-IPN consists of a crosslinked polymer and a linear polymer trapped inside the crosslinked network. Full-IPN includes two crosslinked polymer with physical entanglements [26]. Finally, graft-IPN is similar to full IPN. However, selected chemical bonds between the two polymers are utilized to enhance the compatibility even further [24,27].

IPNs can also be classified into simultaneous and sequential IPNs based on the polymerization method.

In sequential IPNs, the polymerization of the first polymer occurs first, while the monomers of the second polymer swell the system. Once the initial polymerization occurs, the polymerization of the second polymer begins. Simultaneous IPNs are different in that the polymerization of two polymers coincides with no interfering reaction [23,28,29].

Many different research groups, including authors, such as Millar et al. [27] and Frisch et al. [30], studied different aspects of IPNs [12,23,31–37]. Factors such as changing the composition of two polymers, curing profile [38–42], grafting two polymers [43], synthesis method [40], and choice of monomers and catalysts [39], were studied. It was mentioned that utilizing a sequential polymerization method with linear isocyanate rather than aromatic isocyanate, and using chemical bonds, synthesize the IPNs with the best compatibility, and therefore enhancing the transparency and fracture toughness [5,11,40,43–47].

In this research, flexible graft-IPNs out of PU and styrene and MMA based acrylic copolymer were synthesized for the first time. Excellent transparency and impact properties were obtained in all samples. Different properties of the IPNs, such as impact resistance, shear strength, thermomechanical, and tensile strength, were studied. Furthermore, the polymerization reaction between the two networks was analyzed using the FTIR method. The final results confirmed the potential of the synthesized novel flexible IPNs in high-performance applications such as interlayer adhesives in bulletproof transparent applications, windshields, and many other high-performance applications where high transparency, impact resistance, and elastomeric behavior are required.

2. Experimental

2.1. Materials

In this research, the polyurethane phase was synthesized by 2-ethyl-2-(hydroxymethyl)-1,3-propanediol (TRIOL, MW = 134.18 g/mol) as a crosslinker purchased from Acros Organics, poly(tetramethylene ether) glycol (Tetrathane® 1400) (PTMG, MW = 1400 g/mol) donated from Lycra. Hexamethylene diisocyanate (DCH) was purchased from TCI. Moreover, dibutyltin dilaurate (DBTDL) and triphenyl bismuth (TPB) as catalysts were purchased from Pfaltz & Bauer and Alfa Aesar, respectively. Both catalysts were dissolved in ethyl acetate, purchased from Alfa Aesar. Styrene, purchased from Alfa Aesar, Methyl methacrylate (MMA) purchased from Acros Organics, and bisphenol A bis(2-hydroxy-3-methacryloxypropyl) ether (BisGMA), purchased from Esstech, was used to synthesized acrylic copolymer phase. 2,2′-azobis(2-methyl-propionitrile) (AIBN, thermal initiator) was purchased from Matrix Scientific. 4 Å molecular sieves, purchased from Alfa Aesar, were utilized to remove the moisture from DCH, styrene, MMA, TRIOL, and PTMG. Polycarbonate (PC) sheets (3.175 mm and 6.35 mm thickness) were purchased from the US sealing.

3. Methods

3.1. Synthesis of graft-IPNs

For the PU phase, TRIOL and PTMG with 0.19 eq. and 0.12 eq. respectively, were heated and mixed at 60 °C. The mixture was cooled down first, and then 0.31 eq DCH was added.

For synthesis the acrylic copolymer phase, 20 wt% of BisGMA, was dissolved into 80 wt% Styrene or MMA. Then 1 wt% of the total mass of acrylic copolymer, AIBN, was dissolved into the mixture. Afterward, PU and acrylic copolymer monomers were mixed. Finally, 150 μL, 0.02 M ethyl acetate solution of DBTDL, and 75 μL, 0.001 M ethyl acetate solution of TPB per 50 g of PU were added to the monomers to catalyze the poly-addition polymerization of the PU system. The mixture was then

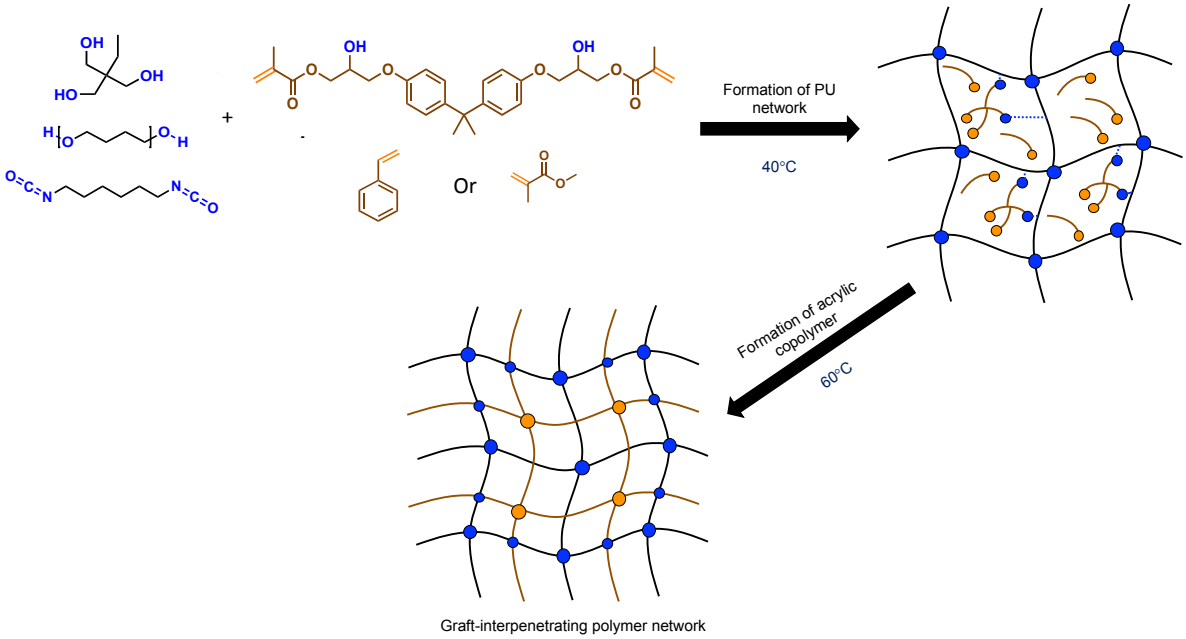

Fig. 1-b. A schematic of the graft-IPN synthesis.

Table 1
Summary of samples made in this research.

Samples	PU (wt %)	Acrylic copolymer (wt%)
PU	100	0
IPN75-Styrene	75	25 (80 wt% Styrene and 20 wt% BisGMA as monomers)
IPN50-Styrene	50	50 (80 wt% Styrene and 20 wt% BisGMA as monomers)
IPN75-MMA	75	25 (80 wt% MMA and 20 wt% BisGMA as monomers)
IPN50-MMA	50	50 (80 wt% MMA and 20 wt% BisGMA as monomers)
COP-Styrene	0	100 (80 wt% Styrene and 20 wt% BisGMA as monomers)

vacuumed under 95 kPa for 5 min, and it was cured at room temperature in closed glass molds, which was increased gradually to reach 40 °C for 24 h, followed by 24 h at 60 °C, and finally 24 h at 80 °C. The schematic of two poly-addition polymerizations happening to synthesize the PU phase and free radical polymerization of a mixture of styrene or MMA and BisGMA are shown in Fig. 1-a and b. Fig. 1-a shows the free radical polymerization of MMA and BisGMA to synthesize acrylic copolymer. Moreover, a simple schematic of the graft-IPN synthesis is shown in Fig. 1-b. The free radical polymerization of Styrene and BisGMA to synthesize acrylic copolymer was shown elsewhere [34].

As shown in Fig. 1-b, the poly-addition polymerization of the PU phase occurs at a lower temperature. The crosslinked polyurethane traps the monomers of the second polymer inside itself. Moreover, the hydroxyl groups of BisGMA started to react with the isocyanate groups to account for the chemical bonds between the two networks. At 60 °C, the thermal initiator of the acrylic copolymer decomposes, starting the free radical polymerization. Samples were post cured at 80 °C to ensure that all of the active groups were reacted in systems. All samples prepared in this research were summarized in Table 1.

3.2. Characterization

Modulated differential scanning calorimetry (DSC) experiment was performed on TA Instruments DSCQ2000. 5 to 10 mg of samples were used for each test. Samples were first equilibrated at −90 °C for 5 min, then heated to 200 °C, cooled to −90 °C, and finally heated to 200 °C with 5 °C/min heating rate in a nitrogen atmosphere.

Thermogravimetric analysis (TGA) was performed on TA Instruments TGAQ500. Between 10 and 20 mg of each sample was placed on a platinum pan and were heated from room temperature to 800 °C with 10 °C/min under a nitrogen atmosphere.

Fourier transform infrared spectroscopy (FTIR) analysis was performed using Nicolet 6700 FTIR spectrometer from Thermo Scientific (US) in attenuated total reflection (ATR) infrared mode. FTIR analysis uses 400–4000 cm^{-1} wavenumber with 64 scans and 4 cm^{-1} resolution.

Thermo-mechanical analysis experiments were performed using TA Instruments RSA 3 dynamic mechanical analyzer (DMA). The flexural test was performed on samples with 35 × 10 × 3 mm and measurements from −100 to 200 °C at 5 °C/min heating rate, with a sinusoidal strain amplitude of 0.5% and 1 Hz frequency, following ASTM E1640 [48]. At least 5 specimens for each sample were tested.

The tensile test was performed using a universal testing machine Instron® 5565 with 1 kN static load cell according to ASTM D638 and Type V dog bone geometry with 63.5 mm overall length, 7.62 mm gage length, 3.18 mm width of narrow section, and ≃ 3 mm thickness [49]. The test was performed under displacement control mode at 10 mm/min. At least 10 specimens were tested for each composition. Boss Laser LS 3655 was utilized to cut cured samples to the desired shape for tensile and DMA tests.

A Zeiss EVO 50 variable pressure scanning electron microscope (SEM) with digital imaging and EDS was utilized to examine the cross-section of the tensile specimens after failure on their gauge. The samples were sputter-coated with an EMS 550X auto sputter coating device with carbon coating attachment.

PC sheets were cut to 152.4 × 152.4 mm squares in preparation for impact-resistant tests. Then IPN monomers were added between two sheets making a sandwich structure. Afterward, 1.2 kg weight was put on the top of the sandwich to keep the PC sheets together and avoid introducing air bubbles between PC sheets. Finally, sandwich structures were cured similarly, as explained in the IPN synthesis section. The impact-resistant test was performed on the Instron® instrumented impact testing machine (Dynatup 8250), following ASTM D5420 [50] (GD geometry) and ASTM D3763 [51]. A mass of 22.58 kg falling from 82 cm height to hit the sample clamped to the platform having a hole of 76 mm by a dart with a hemispherical nose (tup) of 17.6 mm diameter was used for impact-resistant test.

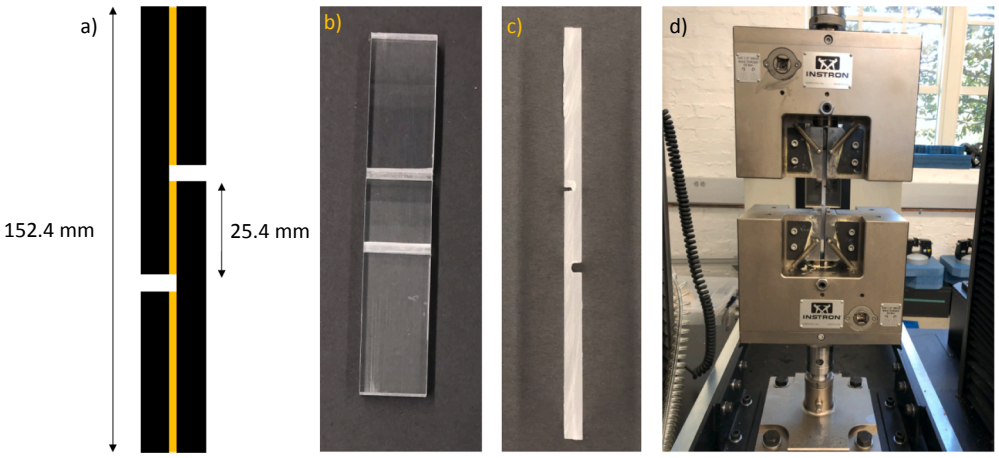

Fig. 2. a) A simple schematic b) Top view and c) cross-section view of samples prepared for lap shear test, d) loaded sample on the tensile instrument.

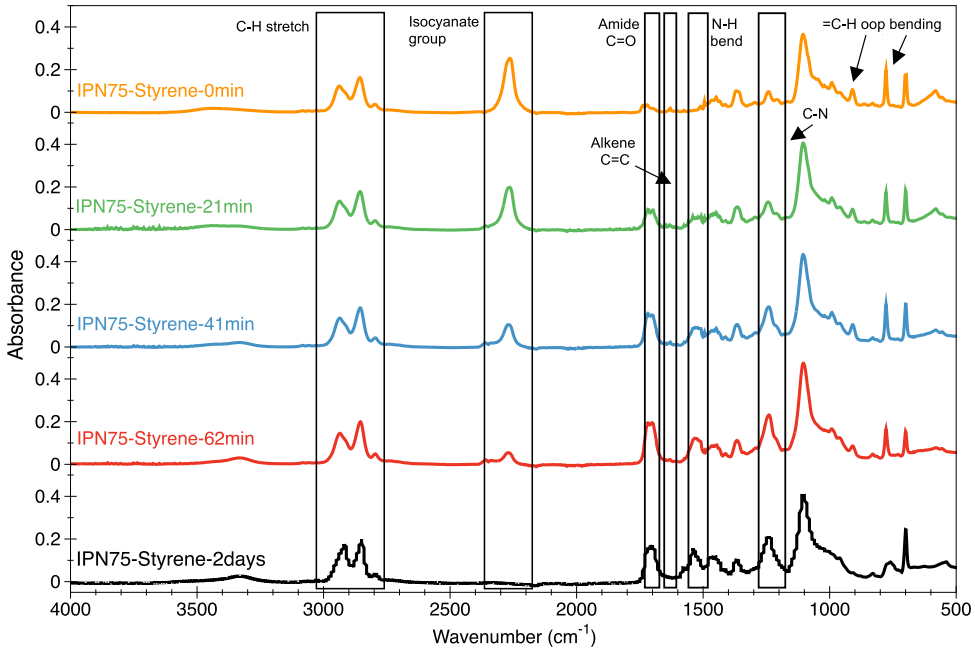

Fig. 3. FTI-IR spectra of IPN75-Styrene at 5 different times.

A Shimadzu UV-2450 spectrometer was used to verify the transparency of the samples (450–800 nm wavelength). For this purpose, similar samples prepared for impact resistance were cut into 25.4 × 25.4 mm with a saw. Moreover, Pure Pc sheets were used as background.

The IPNs strength as an adhesive in shear was performed by tension loading of single-lap-joint assemblies, ASTM D3165 [52]. The samples laminated assembly was prepared a similar procedure followed for preparing impact test samples with regard to putting the IPN monomers between the two layers of 152.4 mm × 152.4 mm squares and cure it. Then sandwich samples were cut into 25.4 × 152.4 mm specimens. Finally, prepared specimens were notched twice at the right angle to the long axis of the specimen at 12.7 mm from the middle of the opposite sides, providing an area of 25.4 × 25.4 mm joint. The notch depth is to cut the sheet and the adhesive material in the thickness direction. Fig. 2. a, b, and c show different views of prepared shear samples, while Fig. 2. d shows the sample loaded into the tensile testing machine, Instron® 5582, with a 100 kN static load cell. The test performed under displacement control mode at 1 mm/min. At least 10 specimens were tested for each composition. Eq. (1) was used to calculate the shear stress of the samples.

$$\tau = \frac{F}{A_0} \tag{1}$$

where τ is the shear stress, F is the maximum force, andA_0 is the initial cross-section.

4. Results and discussion

Heating cycle of DSC experiment indicated no crystallization with a minimum amount of post-curing in all samples, as shown in Figure S1.

TGA analysis was utilized to study the thermal stability of the IPN samples. As shown in Figure S2, the degradation for all samples started at approximately 300 °C and finished at around 450 °C. The degradation temperature obtained from TGA analysis was much higher than the application temperature of IPN samples. PU degraded at a higher rate than other IPN samples due to acrylic copolymer presence, which increased the samples' thermal stability. However, All IPN samples followed the same trend regards to degradation.

The FTIR analysis was utilized to clarify the successful

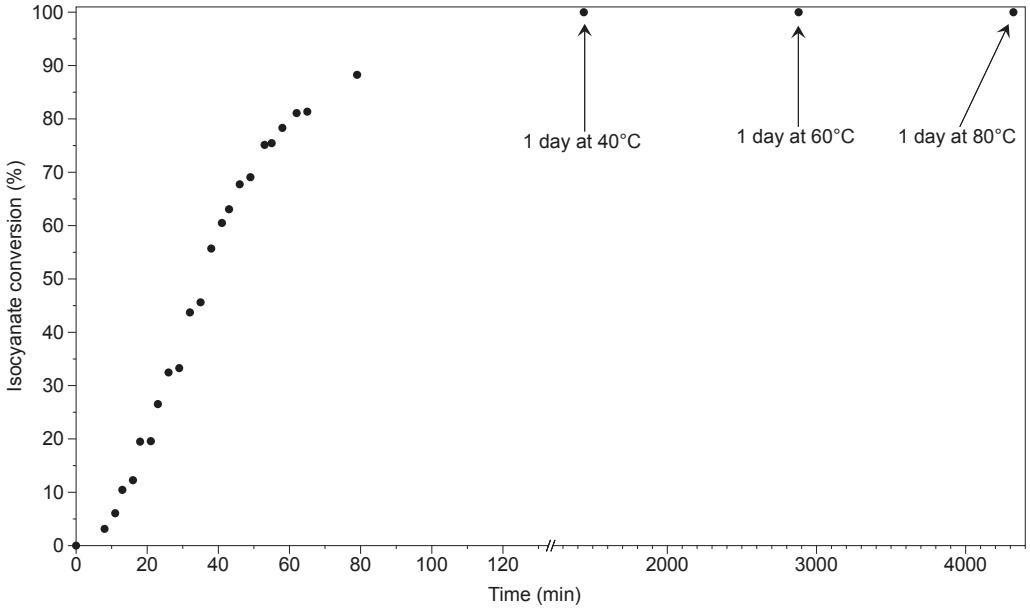

Fig. 4. Isocyanate conversion of IPN75-Styrene.

polymerization of each polymer in IPN systems. FTIR spectra of IPN75-Styrene at 0, 21, 41, 62 min and two days were shown in Fig. 3. As it is shown, the peak around 3454 cm^{-1} belongs to the O-H bond and shift to the lower wavenumber (around 3330 cm^{-1}), which belongs to the stretching of the N-H bond. It confirms the formation of the PU after polymerization. The disappearance of isocyanate (NCO) peak around 2257 cm^{-1} shows the full consumption of the isocyanate group, and it is another evidence for the formation of PU. The formation of amide C═O bond, bending of N-H bond, and C-N bond are other evidence to confirm the successful synthesis of PU. Peaks around 1627 cm^{-1} belong to the alkene C═C bond, which disappears after polymerization. The disappearance of the alkene peak confirms the polymerization of the acrylic phase in the system. Moreover, peaks around 780 cm^{-1} and 910 cm^{-1}, attributed to out-of-plane (oop) bending of ═C-H bonds, disappear in IPN75-Styrene due to the free radical polymerization.

To analyze the isocyanate conversion of flexible IPN material during the polymerization, IPN75-Styrene was chosen. Isocyanate peak, which happens around 2270 cm^{-1}, was monitored during the polymerization while stretching C-H (within 2850–3000 cm^{-1}) was used as standard due to the constant concentration during the polymerization [53]. Eq. (2) [54] was used to calculate the isocyanate conversion.

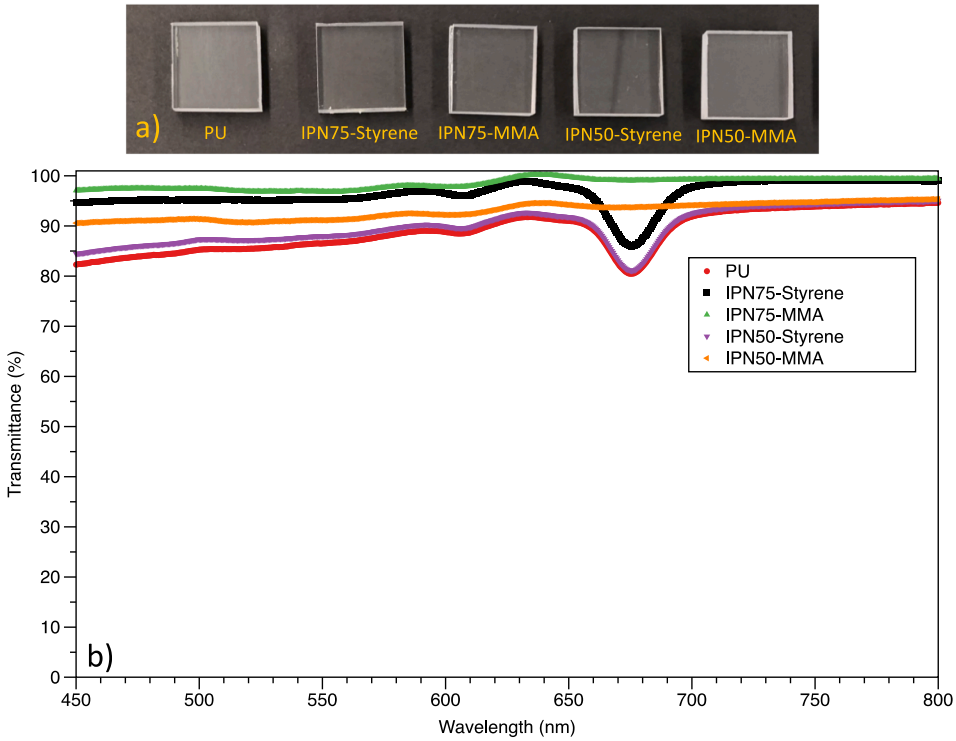

Fig. 5. a) Sandwich structures prepared for transparency test b) UV–Visible spectra of the samples.

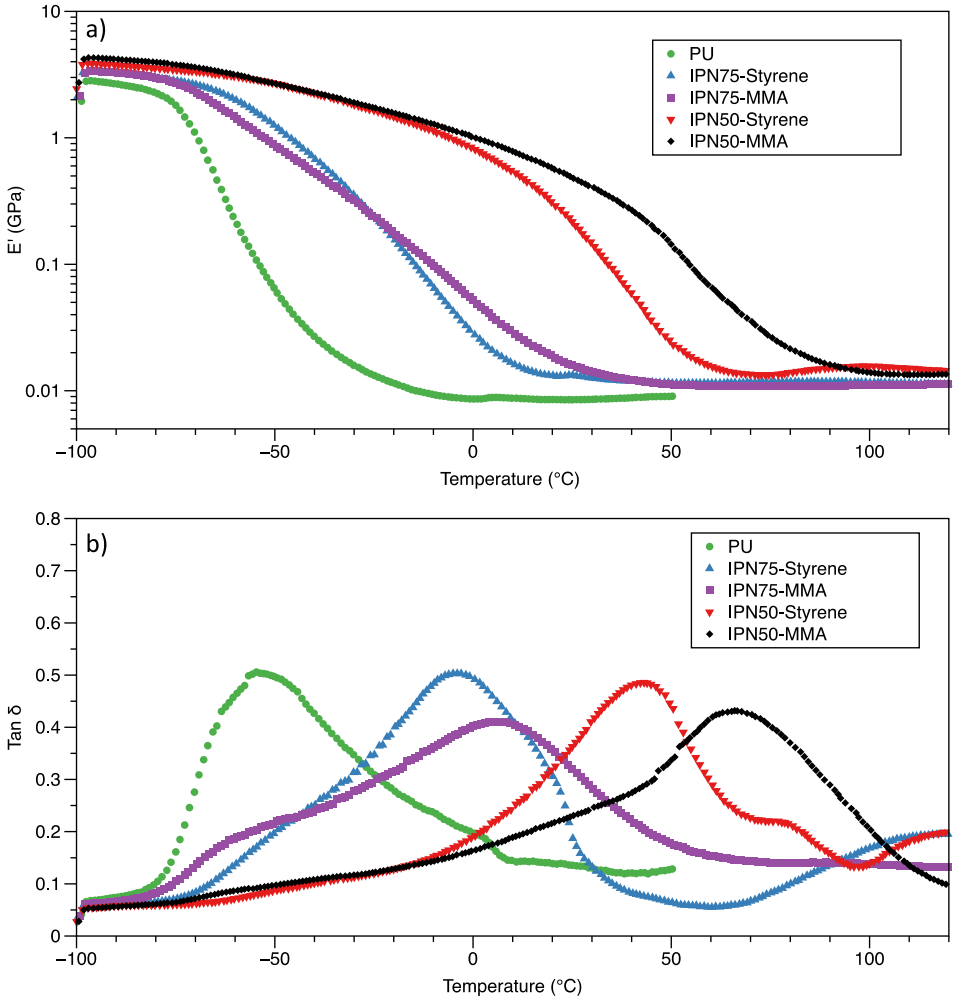

Fig. 6. Thermo-mechanical analysis of materials a) E' vs. Temperature and b) tan δ vs. temperature.

$$p = 1 - \frac{\frac{A_{NCO}}{A_{CH_2}}}{\left(\frac{A_{NCO}}{A_{CH_2}}\right)_0} \quad (2)$$

where p is isocyanate conversion, A_{NCO} is integrated absorbance for NCO peak, A_{CH_2} is integrated absorbance for stretching of C-H peak, and $\left(\frac{A_{NCO}}{A_{CH_2}}\right)_0$ is the relative absorbance extrapolated to time zero.

As shown in Fig. 3, the isocyanate peak at approximately 2270 cm^{-1} starts to decrease during the polymerization due to the reaction between the isocyanate group and a hydroxyl group, which causes the formation of the PU structure. Moreover, the C-H stretch peak remains similar during the polymerization. The result for isocyanate conversion is shown in Fig. 4.

As it is shown in Fig. 4, IPN75-Styrene reaches to 50% of isocyanate conversion approximately after 40 min, and then conversion reaches to 90% after around 90 min. Finally, the conversion becomes 100% at the end of the polymerization process. IPN75-Styrene follows the same trend as rigid IPN with a composition of 75 wt% of copolymer and 25 wt % of PU explained elsewhere [34].

UV–Visible spectrophotometry was utilized to study the transparency of the samples. Fig. 5. shows the sandwich structures (Fig. 5.a), and results of transparency for different samples (Fig. 5.b). As shown in Fig. 5, All IPN samples show transparency higher than 80% in a visible light region. PU shows the lowest transparency in comparison to other samples. Slight tinting in PU structure decreases the transparency of the pure PU samples [7]. Adding more acrylic copolymer into the system increases the transparency of the samples. Furthermore, as it is shown, IPN75 samples show transmittance between 95 and 100%.

Table 2
Summary of thermo-mechanical results.

Sample	Storage modulus E′ (GPa)	T_g (°C)	Tan δ
PU	2.80 ± 1.08	−52.44 ± 2.73	0.49 ± 0.01
IPN75-Styrene	3.16 ± 0.19	−2.80 ± 2.48	0.47 ± 0.05
IPN75-MMA	3.38 ± 0.20	10.74 ± 5.08	0.37 ± 0.04
IPN50-Styrene	3.50 ± 0.56	39.81 ± 2.78	0.43 ± 0.06
IPN50-MMA	3.92 ± 0.34	62.86 ± 3.04	0.44 ± 0.02

Thermo-mechanical characterization of materials was performed by dynamic mechanical analysis (DMA). Fig. 6 and Table 2 show the results for thermo-mechanical characterization. As it is shown, PU shows the lowest storage modulus (E') and glass transition due to the higher flexibility and mobility of the chains in PU structure. Glass transition of the samples and their storage modulus starts to increase by adding copolymer to PU and synthesizing IPN samples. The IPN50 sample shows the highest storage modulus and glass transition temperature due to the presence of 50 wt% copolymer, which restricts the mobility of chains. IPN samples with MMA show higher storage modulus and T_g. Aminolysis reaction between the ester group of PMMA and amine groups of PU, which forms tertiary amine and, as a result, bring higher interpenetration between two polymer phases, is one of the reasons behind better thermomechanical properties in IPN-MMA samples [55].

Moreover, the nucleophilicity of double bonds in the MMA and

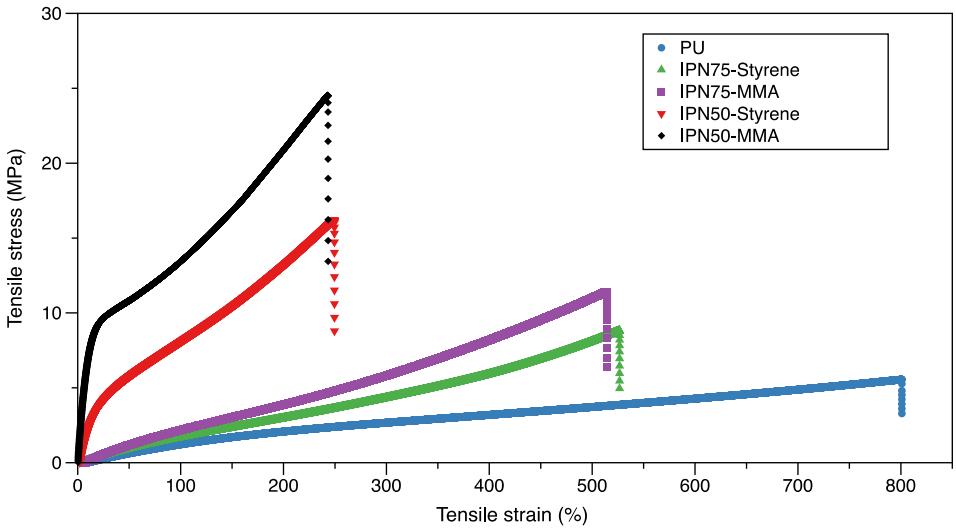

Fig. 7. Tensile analysis of PU and IPN samples.

Table 3
Summary of tensile results for PU and IPN samples.

Sample	Modulus of elasticity (MPa)	Tensile stress at maximum load (MPa)	Tensile strain at maximum load (%)
PU	2.00	5.16 ± 2.49	738.39 ± 360.62
IPN75-Styrene	2.14 ± 0.36	6.12 ± 4.36	332.27 ± 206.43
IPN75-MMA	3.10 ± 0.32	9.01 ± 4.48	440.41 ± 162.72
IPN50-Styrene	19.36 ± 3.85	16.89 ± 3.23	269.64 ± 58.64
IPN50-MMA	86.08 ± 8.79	25.55 ± 3.50	256.23 ± 40.14

BisGMA is relatively similar due to the ester group in their structure, while the nucleophilicity of BisGMA is lower than styrene. Since the ester group in BisGMA has higher electronegativity than the benzene ring in styrene. Accordingly, styrene-based copolymer looks more like an alternating copolymer, and MMA based copolymer looks more like a random copolymer. This fact is another reason for the thermomechanical difference in two different systems [56–58]. Wide storage modulus and glass transition temperature show the potential of synthesized materials in various applications.

Fig. 6.b shows the tan δ vs. temperature of the materials. As it is shown, all materials show a broad tan δ peak due to the several relaxation mechanisms occurring in the system [34,40,43,59]. This fact shows the potential of these materials to be used in damping applications such as shock absorbers and isolators [60]. Moreover, the height of tan δ is another factor in predicting the damping ability of the materials [61]. As shown in Table 2, the height of tan δ starts to decrease by adding more copolymer into the IPN system. This result was expected due to the hindrance provided by acrylic copolymer against chain mobility and therefore reducing the damping ability of the materials.

5. Tensile strength test

All tensile test IPN samples were failed in the gauge section, which shows the validity of the test. Fig. 7 shows the tensile test graphs, while results are summarized in Table 3. As expected, PU shows the highest elongation and lowest tensile stress than other materials due to the higher mobility of the chains in the PU structure. It can be observed that the IPN75 samples show an increase in tensile strength and a decrease in elongation due to the 25 wt% of copolymers into IPN systems.

Table 4
Summary of shear test results for PU, COP-Styrene, and IPN samples.

Sample	Shear stress (MPa)	Tensile strain at maximum load (%)
PU	2.44 ± 0.32	4.10 ± 0.47
IPN75-Styrene	2.20 ± 0.33	2.78 ± 0.38
IPN75-MMA	1.94 ± 0.40	2.54 ± 0.50
IPN50-Styrene	2.13 ± 0.37	2.59 ± 0.51
IPN50-MMA	2.02 ± 0.39	2.46 ± 0.51
COP-Styrene	1.30 ± 0.43	1.57 ± 0.47

Copolymer acts as reinforcements and therefore increases the tensile strength and, at the same time, decreases the flexibility of the samples. Modulus of the elasticity follows the same trend as it increases by adding more COP into the system. Finally, IPN50 samples show the lowest elongation with the highest tensile strength due to the reason mentioned above. PU shows completely elastomeric behavior in the tensile test, while the tensile behavior of IPN samples becomes more ductile by adding more copolymer as reinforcement. IPN-MMA samples exhibit higher modulus and tensile strength in comparison to IPN-Styrene samples due to the aminolysis reaction and different copolymer structures between IPN samples, which was discussed in the DMA section.

The cross-section of the fractured surface area was studied using SEM. Mirror-like surfaces with no specific features were observed for all the analyzed samples, as shown in Figure S3. The flat surface of all the IPN samples with no textured properties, similar to PU surface, is also evidence of good homogeneity with no phase separation between two phases [38].

6. Tensile shear test

All samples were failed in shear through the adhesive. Table 4 shows a summary of the shear results for all the samples. In this experiment, COP-Styrene was used as the reference, which has the highest rigidity in comparison to other adhesive materials. As expected, PU shows the highest shear stress and displacement values due to higher free volume and mobility of the chains in the PU structure. Shear stress value starts to decrease by synthesizing IPN samples out of PU. Reduction in the amount of PU in the system and the presence of acrylic copolymer into the system, which acts as a hindrance against free movement of polymer chains, are the reasons behind the decrease in shear stress. Surprisingly, IPN75-MMA shows smaller shear stress and displacement in comparison to IPN-50 samples. However, as is shown in Table 4. the difference is not considerable for IPN samples. Finally, COP-Styrene shows the lowest

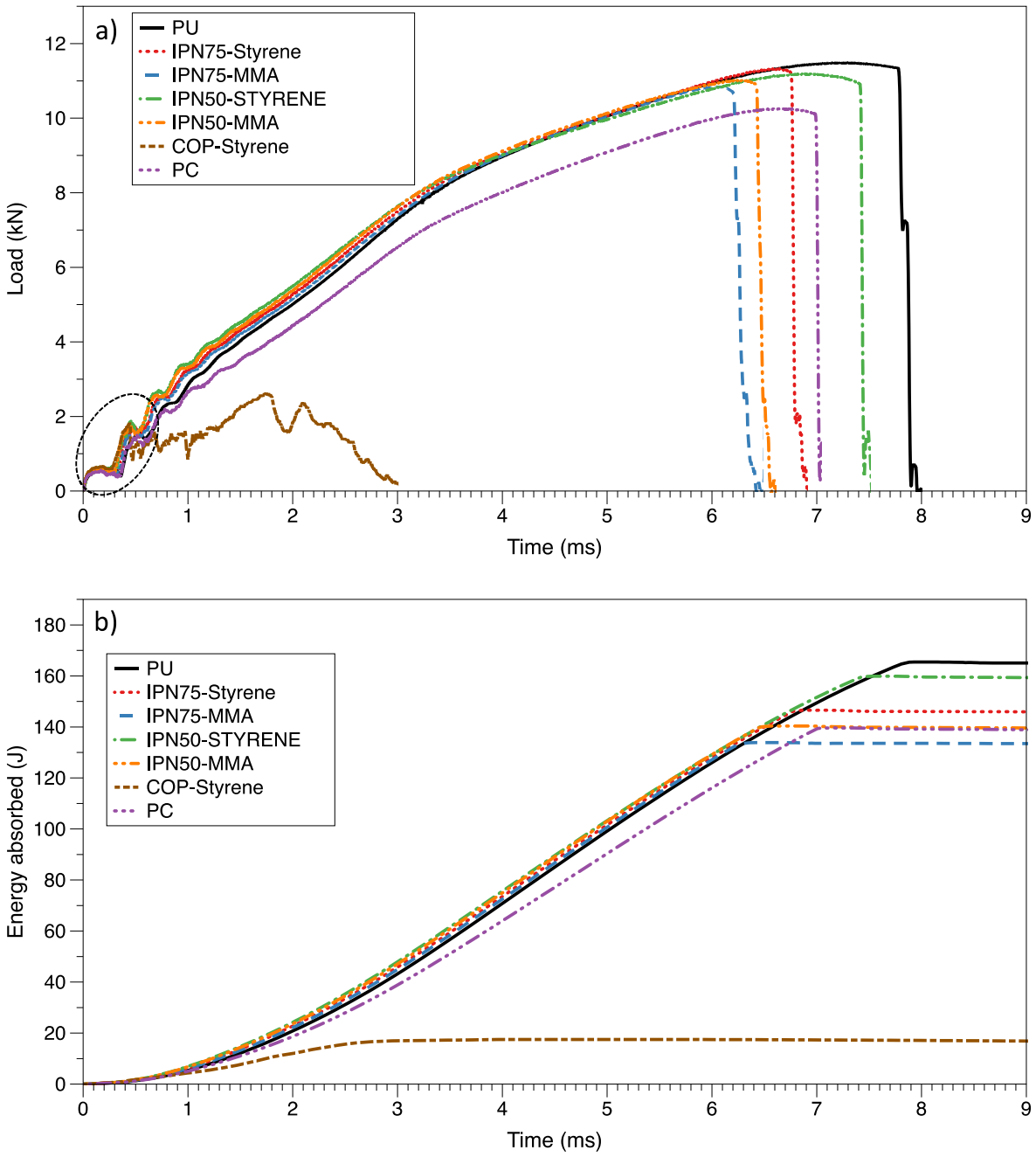

Fig. 8. Impact resistance results a) Load vs. Time b) Energy absorbed vs. Time.

displacement and shear stress due to the low free volume and less mobility of the chains in the acrylic copolymer structure.

7. Impact resistant

The impact-resistant graphs for sandwich structures and a pure PC with similar thickness are shown in Fig. 8 and summarized in Table 5. Initially, force fluctuation was observed in all samples, as shown within the dotted ellipse (Fig. 8.a). The initial force fluctuation occurred due to the initial contact of the striker and the sample's surface. Elastic deformation, followed by elastic reflection, is the reason for the initial fluctuation. Next, the striker penetrates the sample and continues forming a neck shape on the other side. The slope of the load vs. time curves follows similar trends with approximately a similar slope for all samples. It shows that all samples show the same contact stiffness, determined by the slope of load vs. time curves [62]. It should be noted that the slope of load vs. time curves for pure PC is lower; therefore, it has lower contact stiffness in comparison to IPN sandwich structures. After elastic deformation and yielding, samples show a steep drop in load, indicating that the samples experienced permanent plastic deformations.

Fig. 8. b shows the energy absorbed vs. time for different sandwich samples in the impact test. All samples show the linear region of energy absorption showing the elastic deformation, followed by the plateau, which shows the permanent plastic deformation. From Fig. 8 and Table 5, it could be observed that the PU sandwich sample shows the highest energy absorption, deflection, and time before failure due to the higher mobility and free volume of the chains in the PU structure. All of these factors start to decrease by synthesizing IPN out of PU. As shown, PC sheets with IPN products between them show a little higher energy

Table 5
Summary of impact resistance results.

Sample	Time to max load (ms)	Deflection at max load (mm)	Maximum load (kN)	Energy to max load (J)
PU	7.02 ± 0.26	22.47 ± 0.48	11.37 ± 0.44	149.95 ± 6.81
IPN75-Styrene	6.61 ± 0.33	21.55 ± 0.58	11.17 ± 0.33	141.56 ± 8.33
IPN75-MMA	6.15 ± 0.35	20.67 ± 0.77	10.77 ± 0.22	129.64 ± 8.08
IPN50-Styrene	6.62 ± 0.29	21.45 ± 0.53	11.11 ± 0.45	143.31 ± 7.73
IPN50-MMA	6.18 ± 0.45	20.57 ± 1.00	11 ± 0.28	132.98 ± 10.80
COP-Styrene	1.15 ± 0.44	4.56 ± 1.73	1.69 ± 0.50	4.96 ± 2.92
PC	6.58 ± 0.28	22.12 ± 0.64	10.44 ± 0.37	131.10 ± 7.35

absorption compared to the PC sheets alone. IPN-Styrene sandwich samples show higher energy absorption due to the higher stiffness in IPN-MMA samples coming from aminolysis reaction between the ester group of PMMA and amine groups of PU, and different copolymer structure of IPN samples [55]. COP-Styrene sample shows much lower values of force and energy absorption compared to the pure PC and IPN sandwich structures. This fact shows the applications of these novel graft-IPN systems where high toughness is required. It also shows the capability of these materials to be used as an adhesive with high impact resistance properties. It should be noted that energy absorption is indicative of the toughness of the material, which could be defined as an optimum number for strength and ductility in different materials [38,63].

Fig. 9. shows the photograph of the samples before the test (first row), the top surface after the test (second row), and the bottom surface after the test (third row). As it is shown, all the samples except COP-Styrene show excellent resistance against the strike due to the high toughness coming from PC sheets and IPN samples in between them. The striker made a hole in all of the samples; however, no crack propagation was observed in any of the samples. This fact shows the massive potential of these graft-IPN materials in high toughness applications. COP-Styrene sandwich, however, shows the catastrophic failure. Circular opening with cracks propagating all over samples is evidence of spallation failure mode in this sample.

8. Conclusions

Flexible graft-IPNs were successfully synthesized out of PU and acrylic copolymer. The effect of changing the composition of the two polymers was studied on different strength properties. Two different graft-IPN with two different monomers (Styrene and MMA) in the acrylic copolymer structure were synthesized in this research. Two polymers in the IPN system were grafted to minimize the phase separation and maximize the properties of the graft-IPNs. FTIR analysis confirms the successful synthesis of two phases in graft-IPN. DMA, Tensile, and shear analysis show a wide range of properties from elastomeric properties to more ductile properties. IPN samples with a higher percentage of PU show more elastomeric behavior, while adding more acrylic copolymer into the system changed the behavior to more ductile. Impact analysis shows high toughness impact resistance for IPN sandwich structures. Moreover, shear analysis shows the potential of synthesized IPN to be used as an adhesive. Finally, excellent transparency was observed in all IPN samples. These results indicate the considerable potential of the novel synthesized IPNs in transparent, high impact applications.

Author contributions

The manuscript was written through the contributions of all authors. All authors have given their approval to the final version of the manuscript.

CRediT authorship contribution statement

Nima Alizadeh: Conceptualization, Methodology, Software, Writing - original draft, Investigation. **Eldon Triggs:** Investigation, Data curation. **Ramsis Farag:** Investigation, Data curation. **Maria L. Auad:** Investigation, Conceptualization, Writing - review & editing, Supervision, Funding acquisition, Project administration.

Declaration of Competing Interest

The authors declare that they have no known competing financial interests or personal relationships that could have appeared to influence the work reported in this paper.

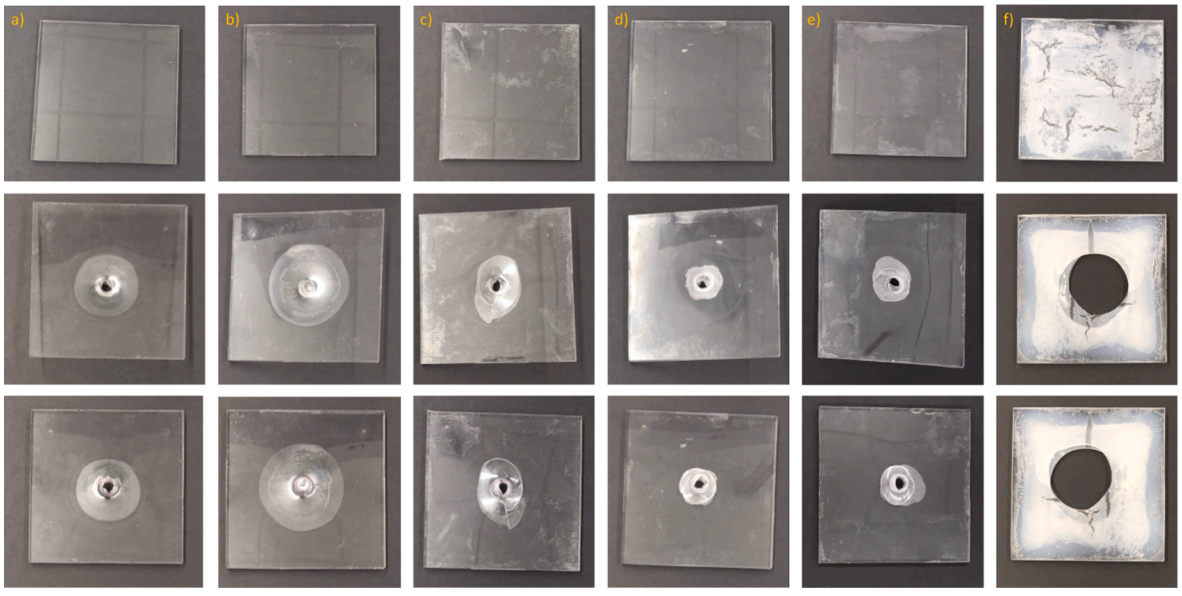

Fig. 9. Photographs of sandwich samples before and after test a) PU b) IPN75-Styrene c) IPN75-MMA d) IPN50-Styrene e) IPN50-MMA f) COP-Styrene.

Acknowledgment

This work was supported by NSF-CREST Center for Sustainable Lightweight Materials (C-SLAM) award #1735971.

Appendix A. Supplementary data

Supplementary data to this article can be found online at https://doi.org/10.1016/j.eurpolymj.2021.110338.

References

[1] H. Holden, To Be a U.S. Secret Service Agent, Zenith Press, 2006.
[2] D.N. Jarrett, Cockpit Engineering, Ashgate Publishing Limited, 2005.
[3] P.J. Hazell, M.R. Edwards, H. Longstaff, J. Erskine, Penetration of a glass-faced transparent elastomeric resin by a lead–antimony-cored bullet, Int. J. Impact Eng. 36 (1) (2009) 147–153.
[4] J.A. Varasdi, Myth Information, Ballantine Books, New York, 1989.
[5] S.A. Bird, Interpenetrating Polymer Networks with Polyurethane and Methacrylate-based Polymers, Polymer and Fiber Engineering, Auburn University, Auburn, AL, 2013, p. 166.
[6] B. Basu, K. Balani, Advanced Structural Ceramics.Hoboken: John Wiley & Sons, Inc., Hoboken: John Wiley & Sons, Inc., 2011.
[7] M. Grujicic, W.C. Bell, B. Pandurangan, Design and material selection guidelines and strategies for transparent armor systems, Mater. Des. 34 (2012) 808–819.
[8] J.E. Girard, Criminalistics: forensic science, crime, and terrorism, second ed., Jones & Bartlett Learning, 2011.
[9] T. Krauthammer, K.A. Marchand, P.F. Mlakar, E.J. Conrath, Structural Design for Physical Security, American Society of Civil Engineers, 1999.
[10] T.F. Scott, W.D. Cook, J.S. Forsythe, Kinetics and network structure of thermally cured vinyl ester resins, Eur. Polym. J. 38 (4) (2002) 705–716.
[11] R.B. Méndez, Sequential graft-Interpenetrating polymer networks based on polyurethane and acrylic/ester copolymers, Polymer and Fiber Engineering, Auburn University, Auburn, AL, 2015, p. 100.
[12] N. Alizadeh, D.P. Thorne, M.L. Auad, A.-D.N. Celestine, Mechanical performance of vinyl ester—polyurethane interpenetrating polymer network composites, J. Appl. Polym. Sci. n/a(n/a) (2021) 50411.
[13] S. Pham, P.J. Burchill, Toughening of vinyl ester resins with modified polybutadienes, Polymer 36 (17) (1995) 3279–3285.
[14] G.Z. Liang, R.L. Zuo, T.L. Lu, J.L. Wang, Modification of vinyl ester resin by a new thermoset liquid crystalline diacrylate, J. Mater. Sci. 40 (8) (2005) 2089–2091.
[15] Z.S. Petrovic, Handbook of polymer synthesis, characterization, and processing, A John Wiley & Sons, Inc., Publication, 2013.
[16] P.J. Patel, G.A. Gilde, P.G. Dehmer, J.W. McCauley, Transparent armour, The AMPTIAC Newsletter 4 (3) (2000).
[17] D.K. Chattopadhyay, K.V.S.N. Raju, Structural engineering of polyurethane coatings for high performance applications, Prog. Polym. Sci. 32 (3) (2007) 352–418.
[18] K.C. Frisch, L.P. Rumao, Catalysis in isocyanate reactions, J. Macromolecular Sci., Part C 5 (1) (1970) 103–149.
[19] S.-G. Luo, H.-M. Tan, J.-G. Zhang, Y.-J. Wu, F.-K. Pei, X.-H. Meng, Catalytic mechanisms of triphenyl bismuth, dibutyltin dilaurate, and their combination in polyurethane-forming reaction, J. Appl. Polym. Sci. 65 (6) (1997) 1217–1225.
[20] L.M. Robeson, Polymer Blends: A Comprehensive Review, Hanser, 2007.
[21] E. Raee, A. Avid, B. Kaffashi, Effect of compatibilizer concentration on dynamic rheological behavior and morphology of thermoplastic starch/polypropylene blends, J. Appl. Polym. Sci. 137 (22) (2020) 48742.
[22] N.P. Panapitiya, S.N. Wijenayake, Y. Huang, D. Bushdiecker, D. Nguyen, C. Ratanawanate, G.J. Kalaw, C.J. Gilpin, I.H. Musselman, K.J. Balkus, J. P. Ferraris, Stabilization of immiscible polymer blends using structure directing metal organic frameworks (MOFs), Polymer 55 (8) (2014) 2028–2034.
[23] L.H. Sperling, V. Mishra, The current status of interpenetrating polymer networks, Polym. Adv. Technol. 7 (4) (1996) 197–208.
[24] L.H. Sperling, D. Klempner, L.A. Utracki, Interpenetrating polymer networks, American Chemical Society, Washington, DC, 1994.
[25] A. Boudenne, L. Ibos, Y. Candau, Handbook of Multiphase Polymer Systems, A John Wiley & Sons Ltd Publication, 2011.
[26] P. Pissis, G. Georgoussis, V.A. Bershtein, E. Neagu, A.M. Fainleib, Dielectric studies in homogeneous and heterogeneous polyurethane/polycyanurate interpenetrating polymer networks, J. Non-Cryst. Solids 305 (1) (2002) 150–158.
[27] L.H. Sperling, Interpenetrating Polymer Networks and Related Materials, Plenum Press, New York, 1981.
[28] L.H. Sperling, Interpenetrating Polymer Networks: An Overview, Interpenetrating Polymer Networks, American Chemical Society, 1994, pp. 3–38.
[29] I. Mita, S. Akiyama, Molecular Design of Network Polymers, in: Macromolecular Design of Polymeric Materials, Marcel Dekker, Inc., 1997.
[30] H.L. Frisch, D. Klempner, K.C. Frisch, A topologically interpenetrating elastomeric network, J. Polym. Sci., Part C: Polym. Lett. 7 (11) (1969) 775–779.
[31] C.H. Chen, W.J. Chen, M.H. Chen, Y.M. Li, Simultaneous full-interpenetrating polymer networks of blocked polyurethane and vinyl ester Part I. Synthesis, swelling ratio, thermal properties and morphology, Polymer 41 (22) (2000) 7961–7967.
[32] L.H. Fan, C.P. Hu, S.K. Ying, Thermal analysis during the formation of polyurethane and vinyl ester resin interpenetrating polymer networks, Polymer 37 (6) (1996) 975–981.
[33] V.J. Dave, H.S. Patel, Synthesis and characterization of interpenetrating polymer networks from transesterified castor oil based polyurethane and polystyrene, J. Saudi Chem. Soc. 21 (1) (2017) 18–24.
[34] N. Alizadeh, M. Barde, M. Minkler, A.-D. Celestine, V. Agrawal, B. Beckingham, M. L. Auad, High fracture toughness acrylic-polyurethane based graft-interpenetrating polymer networks for transparent applications, Polym. Int. n/a(n/a) (2020).
[35] S. Sundararajan, A.B. Samui, P.S. Kulkarni, Interpenetrating phase change polymer networks based on crosslinked polyethylene glycol and poly(hydroxyethyl methacrylate), Sol. Energy Mater. Sol. Cells 149 (2016) 266–274.
[36] B. Sibaja, C.P. Matheus, R.B. Mendez, J.R. Vega-Baudrit, M.L. Auad, Synthesis and characterization of interpenetrating polymer networks (IPNs) from acrylated soybean oil and α-resorcylic acid: Part 1. Kinetics of network formation, J. Renew. Mater. 5 (3–4) (2017) 231–240.
[37] B. Sibaja, C.P. Matheus, R.B. Mendez, R. Farag, J.R.V. Baudrit, M.L. Auad, Synthesis and characterization of interpenetrating polymer networks (IPNs) from acrylated soybean oil α-resorcylic acid: Part 2. Thermo-mechanical properties and linear fracture mechanics, J. Renew. Mater. 5 (3–4) (2017) 241–250.
[38] K.C. Jajam, S.A. Bird, M.L. Auad, H.V. Tippur, Tensile, fracture and impact behavior of transparent Interpenetrating Polymer Networks with polyurethane-poly(methyl methacrylate), Polym. Test 32 (5) (2013) 889–900.
[39] B.M. Sundaram, R.B. Mendez, M.L. Auad, H.V. Tippur, Quasi-static and dynamic mechanical behavior of transparent graft-interpenetrating polymer networks (graft-IPNs), Polym. Test. 70 (2018) 348–362.
[40] S.A. Bird, D. Clary, K.C. Jajam, H.V. Tippur, M.L. Auad, Synthesis and characterization of high performance, transparent interpenetrating polymer networks with polyurethane and poly(methyl methacrylate), Polym. Eng. Sci. 53 (4) (2013) 716–723.
[41] K.C. Jajam, H.V. Tippur, S.A. Bird, M.L. Auad, Dynamic Fracture and Impact Energy Absorption Characteristics of PMMA-PU Transparent Interpenetrating Polymer Networks (IPNs), in: B. Song, D. Casem, J. Kimberley (Eds.) Dynamic Behavior of Materials, vol. 1, Springer International Publishing, Cham, 2014, pp. 277-284.
[42] K.C. Jajam, S.A. Bird, M.L. Auad, H.V. Tippur, Development and Characterization of a PU-PMMA Transparent Interpenetrating Polymer Networks (t-IPNs), in: T. Proulx (Ed.) Dynamic Behavior of Materials, vol. 1, Springer New York, New York, NY, 2011, pp. 117-121.
[43] R. Ballestero, B.M. Sundaram, H.V. Tippur, M.L. Auad, Sequential graft-interpenetrating polymer networks based on polyurethane and acrylic/ester copolymers, Express Polym. Lett. 10(3) (2016) 204-215.
[44] A. Hillerström, M. Andersson, J.S. Pedersen, A. Altskär, M. Langton, J. van Stam, B. Kronberg, Transparency and wettability of PVP/PDMS-IPN synthesized in different organic solvents, J. Appl. Polym. Sci. 114(3) (2009) 1828-1839.
[45] C.-L. Qin, W.-M. Cai, J. Cai, D.-Y. Tang, J.-S. Zhang, M. Qin, Damping properties and morphology of polyurethane/vinyl ester resin interpenetrating polymer network, Mater. Chem. Phys. 85 (2–3) (2004) 402–409.
[46] N. Alizadeh, S.A. Bird, R.B. Mendez, K.C. Jajam, A.C. Alexander, H.V. Tippur, M. L. Auad, Chapter 11 - Synthesis and Characterization of High Performance Interpenetrating Polymer Networks With Polyurethane and Poly(methyl methacrylate), Unsaturated Polyester Resins, Elsevier, 2019, pp. 243–255.
[47] J. Huang, L. Zhang, Effects of NCO/OH molar ratio on structure and properties of graft-interpenetrating polymer networks from polyurethane and nitrolignin, Polymer 43 (8) (2002) 2287–2294.
[48] ASTM E1640-18, Standard Test Method for Assignment of the Glass Transition Temperature By Dynamic Mechanical Analysis, ASTM International, West Conshohocken, PA, 2018.
[49] Standard Test Method for Tensile Properties of Plastics.
[50] Standard Test Method for Impact Resistance of Flat, Rigid Plastic Specimen by Means of a Striker Impacted by a Falling Weight (Gardner Impact).
[51] Standard Test Method for High Speed Puncture Properties of Plastics Using Load and Displacement Sensors.
[52] Standard Test Method for Strength Properties of Adhesives in Shear by Tension Loading of Single-Lap-Joint Laminated Assemblies.
[53] D.L. Pavia, G.M. Lampman, G.S. Kriz, Introduction to spectroscopy, third ed., Thomson Learning, Washington, 2001.
[54] C.A. Cateto, M.F. Barreiro, A.E. Rodrigues, Monitoring of lignin-based polyurethane synthesis by FTIR-ATR, Ind. Crops Prod. 27 (2) (2008) 168–174.
[55] Y. Jin, K.H. Wong, A.M. Granville, Developing localized surface plasmon resonance biosensor chips and fiber optics via direct surface modification of PMMA optical waveguides, Colloids Surf., A 492 (2016) 100–109.
[56] J.R. Fried, Polymer Science and Technology, Prentice Hall Press, New Jersey 07458, 1996.
[57] E.V. Anslyn, D.A. Dougherty, Modern physical organic chemistry, University Science, Sausalito, Calif, 2006.
[58] N.M. Sulca, A. Lungu, C. Zaharia, R. Stan, H. Iovu, Determination of the monomer reactivity ratios in copolymerization of two distinct dimethacrylates for dental use, Mater. Plast. 47 (2) (2010) 254.
[59] M.L. Auad, M. Aranguren, J. Borrajo, Epoxy-based divinyl ester resin/styrene copolymers: composition dependence of the mechanical and thermal properties, J. Appl. Polym. Sci. 66 (6) (1997) 1059–1066.
[60] R. Askarbekov, D. Herak, C. Mizera, Mechanical Behavior of Rubber Samples Under Relaxation, Proceedings of the International Scientific Conference, 2016.

[61] T.M. Wang, S.B. Chen, Q.H. Wang, X.Q. Pei, Damping analysis of polyurethane/ epoxy graft interpenetrating polymer network composites filled with short carbon fiber and micro hollow glass bead, Mater. Des. 31 (8) (2010) 3810–3815.

[62] M.V. Hosur, F. Chowdhury, S. Jeelani, Low-velocity impact response and ultrasonic NDE of woven carbon/ epoxy—nanoclay nanocomposites, J. Compos. Mater. 41 (18) (2007) 2195–2212.

[63] R.O. Ritchie, The conflicts between strength and toughness, Nat. Mater. 10 (11) (2011) 817–822.